Original Article

Investigation of Computed Tomography Numbers on Multiple Imaging Systems using Single and Multislice Methods

Akash Mehta, Daniel Arrington, Prabhakar Ramachandran, Ryan Motley, Venkatakrishnan Seshadri, Darcie Anderson, Margot Lehman, Ben Perrett

Department of Radiation Oncology, Cancer Services, Princess Alexandra Hospital, Woolloongabba, Queensland, Australia

Abstract

Aim: The aim of this study is to determine the variation in Hounsfield values with single and multi-slice methods using in-house software on fan-beam computed tomography (FCT), linear accelerator (linac) cone-beam computed tomography (CBCT), and Icon-CBCT datasets acquired using Gammex and advanced electron density (AED) phantoms. **Materials and Methods:** The AED phantom was scanned on a Toshiba computed tomography (CT) scanner, five linac-based CBCT X-ray volumetric imaging systems, and Leksell Gamma Knife Icon. The variation between single and multi-slice methods was assessed by comparing scans acquired using Gammex and AED phantoms. The variation in Hounsfield units (HUs) between seven different clinical protocols was assessed using the AED phantom. A CIRS Model 605 Radiosurgery Head Phantom (TED) phantom was scanned on all three imaging systems to assess the target dosimetric changes due to HU variation. An in-house software was developed in MATLAB to assess the HU statistics and the trend along the longitudinal axis. **Results:** The FCT dataset showed a minimal variation (central slice ± 3 HU) in HU values along the long axis. A similar trend was also observed between the studied clinical protocols acquired on FCT. Variation among multiple linac CBCTs was insignificant. In the case of the water insert, a maximum HU variation of −7.23 ± 68.67 was observed for Linac 1 towards the inferior end of the phantom. All five linacs appeared to have a similar trend in terms of HU variation from the proximal to the distal end of the phantom, with a few outliers for Linac 5. Among three imaging modalities, the maximum variation was observed in gamma knife CBCTs, whereas FCT showed no appreciable deviation from the central value. In terms of dosimetric comparison, the mean dose in CT and Linac CBCT scans differed by <0.5 Gy, whereas at least a 1 Gy difference was observed between CT and gamma knife CBCT. **Conclusion:** This study shows a minimal variation with FCT between single, volume-based, and multislice methods, and hence the current approach of determining the CT-electron density curve based on a single-slice method would be sufficient for producing a HU calibrations curve for treatment planning. However, CBCTs acquired on linac, and in particular, gamma knife systems, show noticeable variations along the long axis, which is likely to affect the dose calculations performed on CBCTs. It is highly recommended to assess the Hounsfield values on multiple slices before using the HU curve for dose calculations.

Keywords: Advanced electron density phantom, computed tomography-to-electron density phantom, cone-beam computed tomography, fan-beam computed tomography, Gammex

Received on: 14-01-2023 **Review completed on:** 24-02-2023 **Accepted on:** 28-02-2023 **Published on:** 18-04-2023

Introduction

Computed tomography (CT) plays a vital role in radiotherapy treatment simulation and planning. CT scan images are traditionally used as the primary imaging modality for treatment planning due to their acceptable tissue contrast, geometric accuracy, and the ability to correlate their image pixel values (CT numbers) to the linear attenuation coefficients of the materials in the voxel of interest. The CT datasets are useful for tumor localization, contouring of targets and organs at risk, and dose calculations. In general, the aim of treatment planning is to design, prescribe and optimize the radiation dose to the tumor volume while simultaneously minimizing the normal tissue complication probability in nearby healthy tissues. Sophisticated dose calculation algorithms are used to compute the dose on CT images utilizing either relative electron density or physical density information of various tissue materials in the human body. In addition to CT, and

Access this article online

Quick Response Code:

Website: www.jmp.org.in

DOI: 10.4103/jmp.jmp_3_23

Address for correspondence: Prof. Prabhakar Ramachandran, Therapeutic Physics, Radiation Oncology, Cancer Services, Princess Alexandra Hospital, Woolloongabba, Queensland 4102, Australia.
E-mail: prabhakar.ramachandran@health.qld.gov.au

How to cite this article: Mehta A, Arrington D, Ramachandran P, Motley R, Seshadri V, Anderson D, *et al*. Investigation of computed tomography numbers on multiple imaging systems using single and multislice methods. J Med Phys 2023;48:26-37.

depending on the modality and treatment site, magnetic resonance, positron emission tomography, or single-photon emission CT images can also be used in planning.[1,2]

Radiological interactions with tissues in the human body vary between the kilovoltage energies utilized by a CT, and the megavoltage photon energies utilized for radiotherapy treatment. Photon interactions at megavoltage energies are dominated by Compton scattering,[3] while the photoelectric effect is more dominant at kilovoltage energies introducing strong dependence on the mean atomic number (Z) of the voxel. For dose calculations, Hounsfield curves (CT-electron density [CT-ED]) relate CT number (in Hounsfield units [HUs]) to either relative electron density or physical density. Due to the significant Z dependence in CT numbers, calibration curves can only be applied to materials with a similar mean atomic number. Typically, a bilinear calibration curve is obtained with one section similar to soft tissues and the other section analogous to bones.[4]

The treatment planning system utilizes the radiological attenuation properties of tissues obtained from the Hounsfield curve to accurately model and calculate the interactions of radiation beams in the body. The CT-ED relationship is routinely determined by scanning an electron density phantom on a CT scanner. The CT-ED relationship is specific to an individual CT scanner, and photon beam energy (kVp).[5,6] The phantoms used are embedded with multiple cylindrical inserts of known mass and relative electron densities that simulate various tissues encountered in a human body (e.g. lungs, brain, and cortical bone) and a few high-density materials such as titanium and stainless steel that are used in prosthetic materials. The mean HU information of each insert on the central slice is noted and is related to the respective electron density value.[7] There are multiple phantoms available from various vendors that can be used to carry out this task, some of them include PTW Electron density phantom,[8] Pro-RT ED phantom,[9] Sun Nuclear Advanced Electron Density (AED) Phantom,[10] and Gammex RMI 467 tissue characterization phantom.[11] Conventionally, the CT-ED curve is produced based on the average Hounsfield values determined on the central slice of the electron density phantom. However, HU phantoms such as the Sun Nuclear AED phantom can be used to determine the mean Hounsfield value over a finite volume along the longitudinal axis.

Modern linear accelerators are fitted with acquisition-based cone-beam CT (CBCT) units. These CBCT images are used for image-guided setup and localization of patients for radiation treatment. Improvements in image quality of these CBCT images allow verification of delivered dose using deformable registration with planning CT images. These CBCT images have also been used for adaptive radiation therapy.[12] An integrated CBCT unit is also available for the Leksell Gamma Knife Icon to enable fractionated stereotactic radiation therapy (SRT) of intracranial tumors.

A variation in scanning parameters such as tube voltage, current, and field of view, and imaging modalities can influence CT numbers. The location of the insert in the phantom can lead up to 3% of the difference in HU values.[13,14] Different CT protocols can affect the HU values by as much as 20%.[15] Geometrically identical CBCT scanners equipped with the same flat-panel detectors can have large inter-scanner variations. In addition to this, the size of the scanned object and the amount of scattering can also affect HU values.[16] However, a few studies show that the CBCT-based treatment plans were comparable to CT-based treatment plans.[17,18] A recent paper[19] published in the Radiation Oncology Journal demonstrates that cone-beam CT acquired on the gamma knife is prone to show significant variation along the longitudinal and transverse planes. Before the use of any imaging modality for radiation dose calculation, it is highly recommended to assess variations of the Hounsfield values in different positions representative of the configuration and geometry of the imaging system. In this study, we aim to determine the variation in Hounsfield values with single and multislice methods using Gammex, and AED phantoms on fan-beam CT (FCT), X-ray volumetric imaging (XVI)-based CBCT, and Icon-CBCT datasets. This study also focuses on differences in HU numbers in the longitudinal direction.

Materials and Methods

Investigations were performed to assess the effect of longitudinal variations in HU number on measurements of single slice and volumetric HU values for particular materials. The Toshiba Aquilion CT was used to acquire images to assess longitudinal variations and stability in HU numbers with respect to clinical FCT protocols. A comparison of five linear accelerator (linac) based CBCTs was performed to assess longitudinal variations in HU number and variations between units. A comparison of multiple modalities that include (i) the FCT, (ii) linac-based CBCT, and (iii) the Leksell Gamma Knife (LGK) Icon CBCT was performed to assess the variation in HU numbers. Dose calculations were compared and contrasted using datasets from each modality with corresponding HU calibration curve.

Advanced Electron Density Phantom and Gammex RMI Phantom

The Sun Nuclear AED Phantom is constructed of energy-matched CT Solid Water HE consisting of 14 solid inserts in addition to two containers filled with liquid water. The phantom is 16.6 cm thick and can be extended to 26.5 cm with extension plates. The phantom is split into two interlocking modules to simulate pelvis and head anatomies. The phantom also includes a convenient mounting frame that enables easy assembly and reproducible setup. The Gammex RMI Tissue Characterization Phantom is made of Solid Water® and is 33 cm in diameter and 5 cm longitudinally. It has provisions to hold 16 inserts, including one true water container. The investigation involved utilizing the AED phantom to study different methods of HU determination, along with the Gammex RMI 467 Tissue Characterization Phantom. The phantoms were imaged on the

Toshiba Aquilion 16-slice CT simulator and the kV CBCT XVI units on five Elekta Infinity and Synergy linacs. The AED head phantom was also scanned on all three systems, the FCT, CBCT and Leksell Gamma Knife Icon, to assess the variation between imaging systems.

Software for analyzing Hounsfield unit values

The analysis of phantom image datasets was performed using an in-house developed MATLAB program. This program calculates the minimum, maximum, and mean HU values along with standard deviations over a specified volume.

The user inputs the approximate center positions of each rod on a single slice in the dataset. This is used to generate the analysis region over the specified volume. The program provides a CT DICOM image viewer with tools to scroll through slices and adjust image contrast. Electron density inserts are identified by user input of the central position of individual inserts. Regions of interest (ROIs) can be repositioned with dynamic updates to the displayed results. The software provides optional display of calculated values and statistics on single slices. These individual slice results can be compared against the global volumetric mean values. The software input and results windows are illustrated in Figure 1. The software will be available upon request.

The extracted volume mean and standard deviation results for multiple inserts were validated against the Sun Nuclear RapidCHECK phantom analysis software. For each defined volume, a list of applicable inserts is provided under the description column which automatically updates both the physical density table and the HU plot. The software also has the provision to add additional inserts as required. The individual slice statistics for each volume analyzed are displayed in the top right section of the software, as shown in Figure 1. The table can be exported as a Microsoft Excel spreadsheet, with volumetric results and individual slice statistics for each volume as separate worksheets. In addition to the features available in the RapidCHECK software, the in-house software can plot the mean HU along with standard deviation determined at each slice in the long / lateral / vertical axis.

Variation of Hounsfield unit with respect to longitudinal distance in fan-beam computed tomography

An assessment was performed on the variation of HU numbers including mean and standard deviation for the available inserts in the AED phantom with scans performed using the Toshiba Aquilion CT scanner. The results were compared to the central slice mean and standard deviation values for the inserts in the Gammex RDI 467 Tissue Characterization Phantom. All scans were performed using the Pelvis CT protocol as defined with 120 kVp. The insert configuration for this study is shown in Figure 2.

The length of the inserts in the AED can be utilized to calculate mean HU values for the entire insert volume over multiple image slices as opposed to a single slice as required when using the Gammex phantom. The HU values for each insert were tabulated from both phantoms for comparison of the two methodologies. The analysis was performed using the in-house phantom analysis program.

Hounsfield unit dependency on fan-beam computed tomography acquisition protocol

The influence of FCT acquisition parameters on HU values generated by the in-house software was analyzed by scanning the AED phantom on the Toshiba Aquilion CT simulator. The phantom was imaged using 7 clinical acquisition protocols that include abdomen, chest, head and neck, head and neck ("Sure Exposure"), legs, pelvis, and SRT brain with 120 kVp.

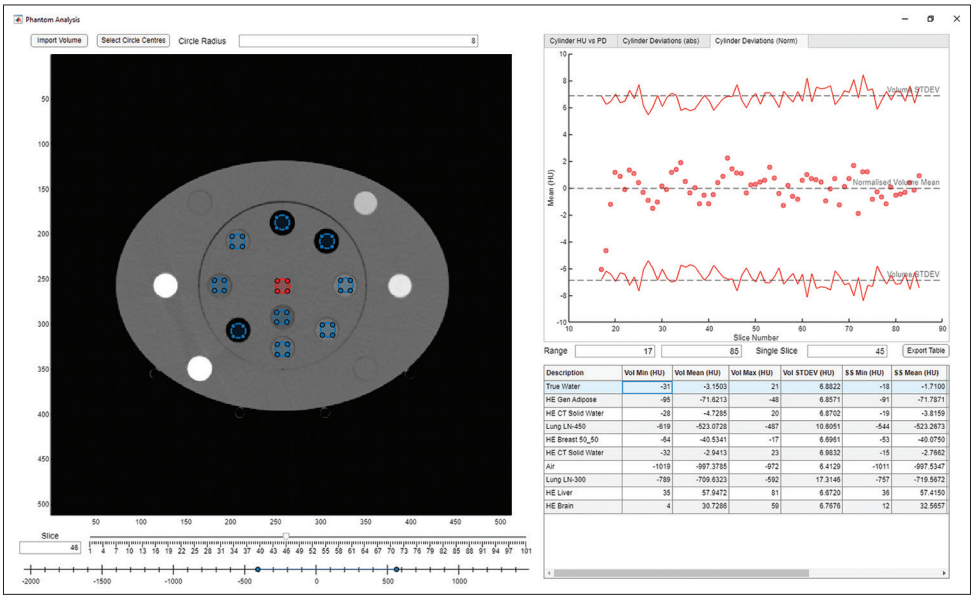

Figure 1: In-house phantom analysis program. It allows the user to select modules and ranges for HU analysis and provides tools to visualize and export the data. HU: Hounsfield unit

Comparison of linac cone-beam computed tomography

The HU variation between XVI linac-mounted CBCTs was assessed by scanning the AED phantom in the configuration as found in Figure 2. Scans were performed on each of the five linac-mounted CBCTs. The scan protocol utilized the large field of view with collimator L20 and bowtie filter (F1). The peak tube potential was set to 120 kVp, with nominal current and exposure time values per frame of 80 mA and 40 ms, respectively. The treatment delivery was performed at 180°/min in a clockwise direction, nominally delivering 660 image frames. Analysis was performed using the in-house software.

Imaging modality comparison

The variations in HU values across different imaging modalities used in radiation therapy were compared and contrasted. This was achieved by scanning the AED phantom on the Toshiba Aquilion CT simulator, the XVI kV CBCT units on an Elekta Infinity Linac, and the kV CBCT unit on Leksell Gamma Knife Icon. Analysis was performed over the region of the phantom where HU values in all inserts are not affected by the phantom edge or the identifying marks in each insert. The scan range performed for CBCT image was also limited by the width of the cone beam. The images were acquired using the clinical protocols on the FCT unit, XVI CBCT unit, and on the kV CBCT (6.3 mAs) of LGK Icon system. The acquisition parameter details are provided in Table 1.

Dosimetric comparison

A comparison was made by assessing the impact that HU value variation across modalities had on the HU curves. To do so, a CIRS Model 605 Radiosurgery Head Phantom (TED) was imaged for 2 mm slice thickness using each of the three modalities. A 7 cm diameter in the axial plane was delineated to define a volume of approximately 106 cc. A plan was created in Pinnacle TPS with four beams spaced at 90° (box-technique) being delivered to a generic planned target volume (PTV) on the FCT dataset. Image fusion was performed and the PTV contour was transferred onto the coordinate system of the linac-based CBCT and the Leksell Gamma Knife Icon CBCT. Markers representing beam orientations were also transferred to each dataset. This information was then used to reconstruct the plan geometry using the linac-based CBCT and the Leksell Gamma Knife Icon CBCT datasets for dose calculation. A dose of 50 Gy was prescribed to the isocenter. Couch, gantry, and collimator angles were adjusted to generate a consistent plan on all three datasets [Figure 3]. The dose was normalized to the isocenter, and the dosimetry was assessed by examining the HU values, volumes, and dose statistics.

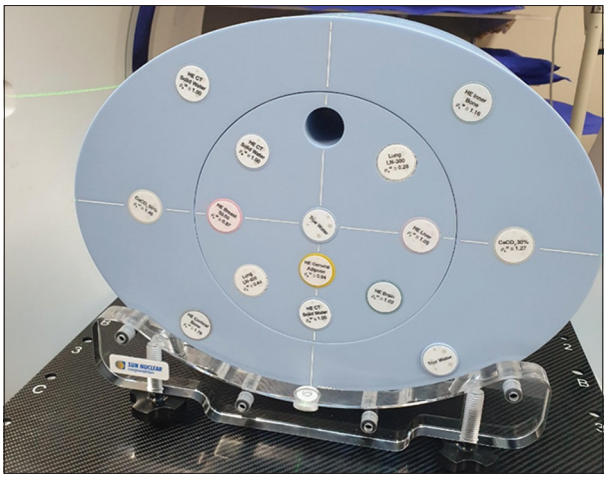

Figure 2: Insert configuration of the AED Phantom. AED: Advanced Electron Density

Results

Variation of Hounsfield unit with respect to longitudinal distance in fan beam computed tomography

The variation in mean HU values for multiple slices along the longitudinal axis of the AED phantom in CT for water, lung and cortical bone inserts is shown in Figures 4-6, respectively. In each case, the blue triangle represents the mean HU value of the respective insert at the center of the phantom scan length whereas the mean HU variation along the phantom with 2 mm increment is shown with orange crosses. In addition to this, red dotted lines illustrate ± 1 σ for each data point. The abscissa illustrates the scanned length of the phantom in millimeters, with zero representing the bottom side of the phantom (superior end). On the other hand, mean HU is plotted along the ordinate indicating the mean HU values of each insert along the axial direction (i.e., in superior-inferior direction).

In the case of the water insert [Figure 4], the mean HU value at the center of the phantom scan length was found to be − 4.8 ± 10.3. An insignificant variation was observed along the axial axis of the phantom with maximum and minimum of −1.74 ± 11.51 (at 72 mm) and − 7.83 ± 11.27 (at 112 mm), respectively. Standard deviation (1 σ) was calculated to be fairly consistent along the scanned phantom with an average of 11.37 ± 0.75. In the case of Lung LN-450 insert [Figure 5], the mean HU values seemed to fluctuate randomly along the axial direction of the scanned phantom without presenting any correlation between mean HU and axial distance. The average HU at the center of the phantom was found to

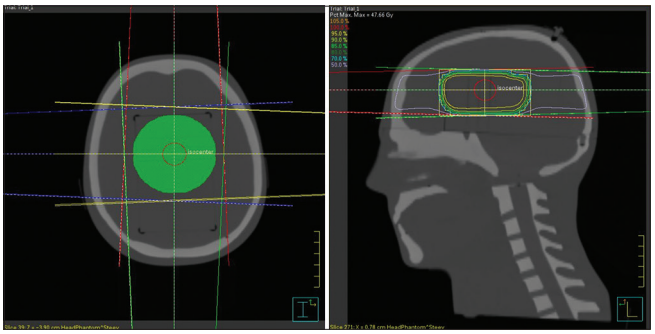

Figure 3: Transverse and sagittal view of the TED head phantom (Green: PTV, Red: Isocenter) – Simple four-field box technique

Table 1: Advanced electron density phantom inserts and mean Hounsfield unit value

Sun nuclear AED phantom				
Inserts	**Physical density (g/cm³)**	**Relative electron density**	**Central slice, mean±SD**	**Multi-slice, mean±SD (range)**
Air	-	-	−995.15±8.4	−995.62±8.4 (−1022-−962)
Lung LN-300	0.295	0.285	−710.92±19.49	−709.16±19.24 (−802-−592)
Lung LN-450	0.484	0.468	−521.55±13.37	−521.94±13.62 (−633-−472)
HE gen adipose	0.959	0.949	−73.41±11.46	−73.43±11.4 (−111-−36)
HE breast 50:50	0.984	0.971	−42.77±10.87	−42.9±11.23 (−80-−2)
True water	1	1	−4.80±10.29	−5.11±11.43 (−49-36)
HE CT solid water	1.019	0.995	−1.31±8.3	−4.37±10.45 (−38-32)
HE brain	1.05	1.024	28.82±10.54	28.18±10.85 (−17-70)
HE liver	1.08	1.054	54.72±10.99	54.77±11.27 (15-93)
HE inner bone	1.214	1.163	314.41±8.45	313.96±8.31 (277-346)
CB2 + 30% $CaCO_3$	1.332	1.268	464.37±9.87	464.58±10.11 (427-506)
CB2 + 50% $CaCO_3$	1.561	1.464	841.42±11.27	841.55±11.32 (793-880)
HE cortical bone	1.923	1.774	1406.33±12.51	1405.02±12.33 (1363-1445)

AED: Advanced electron density, CT: Computed tomography, SD: Standard deviation

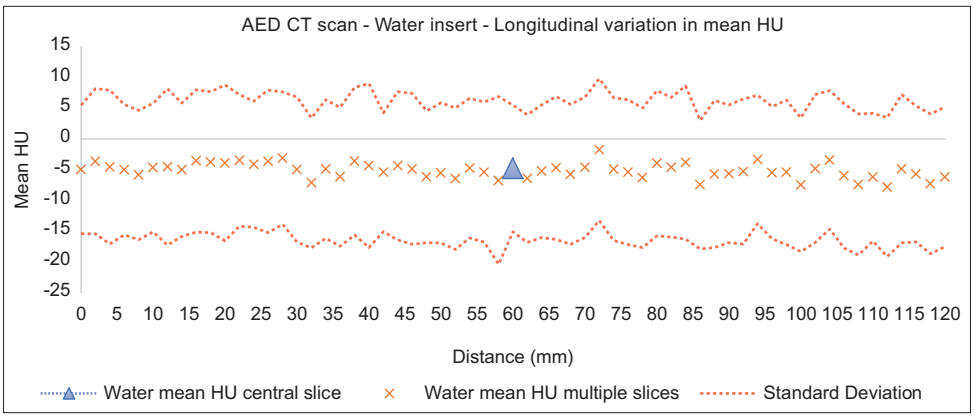

Figure 4: Variation in HU values of water insert along the longitudinal axis of the Sun Nuclear AED phantom. AED: Advanced electron density. HU: Hounsfield unit

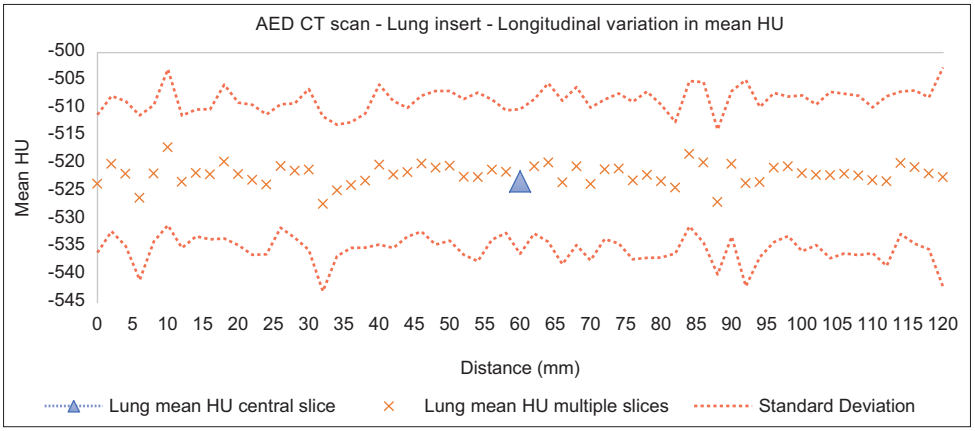

Figure 5: Variation in HU values of lung insert along the longitudinal axis of the Sun Nuclear AED phantom. AED: Advanced electron density, HU: Hounsfield unit

be − 523.2 ± 12.9. The highest variation was noted at 10 mm away from the superior end of the phantom with a mean HU value of −517.1 ± 14.0 and lowest of − 527.2 ± 15.8 in the same direction at 32 mm.

For the cortical bone insert, the mean value at the center of the phantom was measured to be 1405.7 ± 11.9. The HU values did not vary significantly along the phantom with minimum and maximum values of 1400.3 ± 12.5 and 1408.3 ± 11.9,

respectively. Both of these values were at the opposite ends of the phantom, the maximum value was 24 mm away from the superior end whereas the superior end of the phantom corresponded to the minimum value.

In addition to this, all-inserts HU data was also collected for the Gammex RDI 467 tissue characterization phantom and the AED phantom including their physical and relative electron densities as shown in Tables 1 and 2, respectively. A few of the inserts were found to have different physical and relative electron densities for the same corresponding materials between the phantoms, for example, adipose, liver and cortical bone. This variation in the densities resulted in differences in HU values measured for these inserts in their respective phantoms. For AED inserts HU measurements, volume analysis was also performed to estimate the relation between central slice and volume-based HU readings. As shown in Table 1, no significant differences were observed.

Hounsfield unit dependency on fan beam computed tomography acquisition protocol

Table 3 illustrates the volume mean HU analysis of each insert conducted for a number of clinical protocols. The results demonstrate minimal differences (±6 HU) between the mean HU values across the studied protocols.

Comparison of Linac cone-beam computed tomography

The variations in mean HU values for multiple slices along the longitudinal axis of the AED phantom for Linac CBCTs measured for water, lung, and cortical bone inserts are shown in Figures 7-9, respectively. In each case, the blue triangle represents the mean HU value of respective insert at the center of the phantom scan length whereas mean HU variation along the phantom with 2 mm increment is shown with orange crosses, red dots, green diamonds, dark-green squares, and purple stars for Linac 1, 2, 3, 4, and 5, respectively. The abscissa illustrates the scanned length

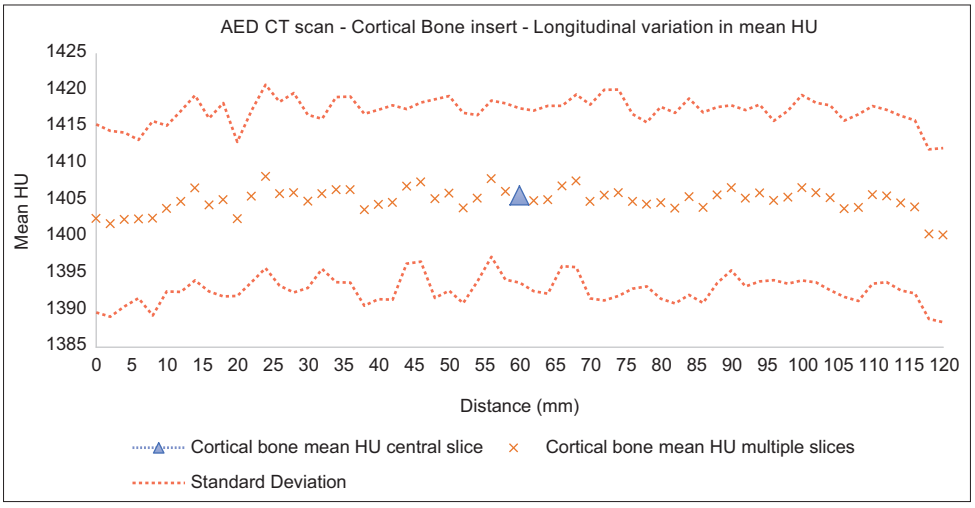

Figure 6: Variation in HU values of cortical bone insert along the longitudinal axis of the Sun Nuclear AED phantom. AED: Advanced electron density. HU: Hounsfield unit

Table 2: Gammex phantom inserts and mean Hounsfield unit values

Gammex RMI 467 tissue characterization phantom			
Inserts	**Physical density (g/cm³)**	**Relative electron density**	**Central slice, mean±SD**
Air	-	-	-
LN-300 lung	0.29	0.286	−716.17±9.9
LN-450 lung	0.48	0.463	−529.35±13.4
AP6 adipose	0.942	0.925	−96.8±11.3
BR-12 breast	0.979	0.956	−49.08±13.8
True water	1	1	−2.6±13.4
CT solid water	1.02	0.991	-
BRN-SR2 brain	1.053	1.049	22.34±12.3
LV1 liver	1.095	1.063	76.6±13.4
IB inner bone	1.140	1.093	212.57±13.1
CB2-30% $CaCO_3$	1.334	1.279	471.38±13.8
CB2-50% $CaCO_3$	1.562	1.472	840.41±14.2
SB3 cortical bone	1.824	1.696	1253.74±15.7

CT: Computed tomography, SD: Standard deviation

Table 3: Clinical computed tomography protocols for various treatment sites

Inserts	FCT protocols					
	Abdomen volume, mean±SD (range)	Chest volume, mean±SD (range)	Head and neck volume, mean±SD (range)	Head and neck "sure exposure" volume, mean±SD (range)	Pelvis volume, mean±SD (range)	Legs volume, mean±SD (range)
Air	−995.94±8.5 (−1029-−969)	−995.82±8.51 (−1027-−960)	−997.51±6.43 (−1019-−972)	−997.35±5.89 (−1022-−976)	−995.56±8.37 (−1022-−967)	−996.35±8.68 (−1024-−967)
Lung LN-300	−709.45±19.39 (−801-−588)	−709.41±19.43 (−805-−581)	−711.62±16.12 (−786-−629)	−709.83±17.36 (−781-−593)	−709.18±19.36 (−802-−592)	−709.66±19.46 (−791-−584)
Lung LN-450	−522.36±13.69 (−633-−480)	−522.18±13.67 (−636-−479)	−522.76±10.45 (−600-−487)	−522.89±10.49 (−616-−485)	−521.96±13.67 (−633-−472)	−522.57±13.93 (−638-−475)
HE gen adipose	−73.45±11.32 (−111-−34)	−73.42±11.45 (−118-−31)	−71.46±6.81 (−95-−48)	−71.94±6.59 (−95-−48)	−73.48±11.39 (−111-−36)	−73.82±11.66 (−110-−26)
HE breast 50_50	−42.53±11.36 (−84-−1)	−42.39±11.19 (−77-−3)	−40.48±6.75 (−64-−17)	−41.2±6.64 (−66-−18)	−42.82±11.24 (−80-−2)	−43.39±11.75 (−87-−4)
True water	−5.36±11.4 (−49-39)	−5.74±11.61 (−49-31)	−3.29±7.03 (−31-21)	−3.55±6.93 (−33-21)	−5.05±11.44 (−45-36)	−6.32±11.56 (−48-32)
True water	−1.09±8.13 (−31-32)	−0.97±8.05 (−29-32)	0.06±6.27 (−30-21)	0.18±5.73 (−42-23)	−1.32±8.22 (−31-26)	−0.96±8.27 (−37-27)
HE CT solid water	−6.59±10.64 (−45-28)	−6.45±10.73 (−42-28)	−4.81±6.9 (−28-20)	−4.7±6.64 (−25-17)	−6.41±10.58 (−47-32)	−6.82±10.91 (−41-30)
HE CT solid water	−4.27±10.38 (−41-36)	−4.3±10.63 (−39-36)	−2.91±6.99 (−32-23)	−2.99±6.51 (−26-18)	−4.38±10.48 (−38-32)	−5.39±10.79 (−41-31)
HE CT solid water	−4.8±7.72 (−35-24)	−4.71±7.65 (−30-20)	−4.73±6.02 (−29-18)	−4.81±5.42 (−22-13)	−5.06±7.72 (−31-28)	−6.22±7.82 (−32-22)
HE brain	28.55±10.82 (−11-65)	28.45±11 (−7-69)	30.73±6.77 (4-59)	30.64±6.36 (10-57)	28.16±10.84 (−17-70)	27.94±11.33 (−18-66)
HE liver	55.07±11.4 (18-99)	55.06±11.39 (12-92)	58.01±6.67 (35-82)	57.48±6.6 (32-85)	54.99±11.29 (15-93)	54.75±11.63 (15-95)
HE inner bone	314.05±8.26 (285-347)	314.19±8.29 (282-343)	315.9±6.33 (293-340)	315.83±5.92 (296-338)	314.26±8.28 (277-346)	313.62±8.63 (278-341)
CB2 + 30% $CaCO_3$	464.73±10.53 (427-503)	465.11±10.43 (427-511)	469.43±6.93 (444-495)	469.01±6.55 (441-493)	464.72±10.16 (427-506)	464.78±10.71 (429-507)
CB2 + 50% $CaCO_3$	842.11±11.51 (802-880)	842.37±11.32 (801-883)	847.88±7.38 (820-877)	846.85±7.15 (820-874)	841.73±11.39 (793-885)	840.93±11.49 (795-883)
HE cortical bone	1405.91±12.27 (1356-1448)	1407.61±13.3 (1349-1459)	1413.62±9.27 (1383-1455)	1412.86±9.55 (1382-1451)	1405.87±12.84 (1363-1455)	1403.75±12.84 (1360-1448)

CT: Computed tomography, SD: Standard deviation, FCT: Fan-beam CT

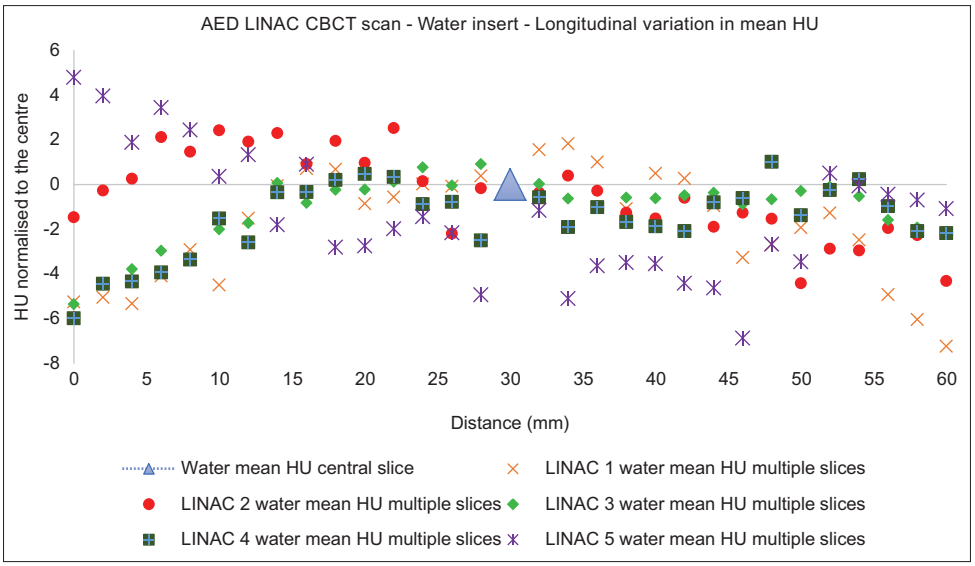

Figure 7: Variation in the Linac CBCT HU values of water insert along the longitudinal axis of the AED phantom. CBCT: Cone-beam computed tomography, AED: Advanced electron density, HU: Hounsfield unit

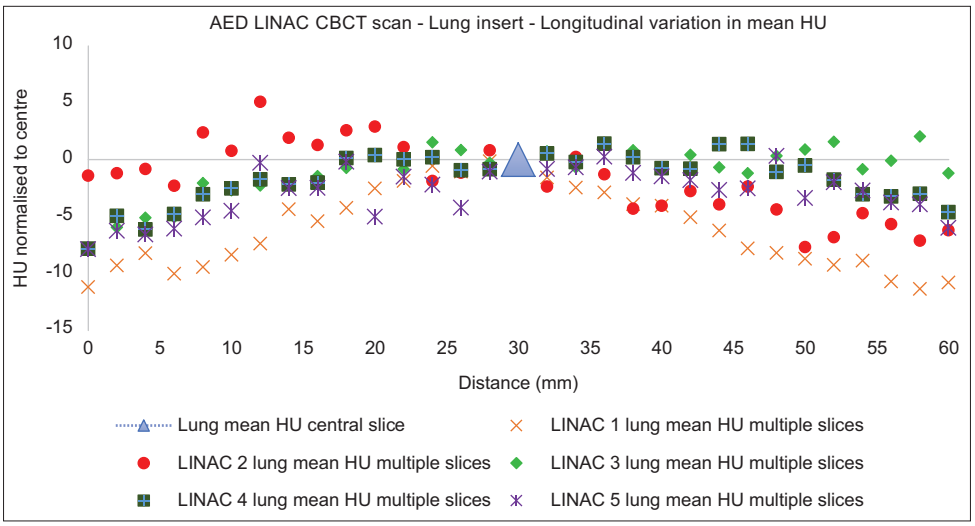

Figure 8: Variation in Linac CBCT HU values of Lung insert along the longitudinal axis of the AED phantom. CBCT: Cone-beam computed tomography, AED: Advanced electron density, HU: Hounsfield unit

of the phantom in millimeters, with zero representing the bottom side of the phantom (superior end). On the other hand, mean HU (normalized to the reading at the center of scanned part of the phantom per individual Linac) is plotted along the ordinate indicating the normalized HU values of each insert along the axial direction (i.e., in superior-inferior direction).

In the case of the water insert, a maximum HU variation of -7.23 ± 68.67 was observed for Linac 1 toward the inferior end of the phantom. As shown in Figure 7, the variation decreased towards the center of scanned phantom. It also tends to vary in a similar random fashion when analyzed in the other half of the phantom (inferiorly). Similar changes were observed in other Linac CBCTs with different magnitudes of variation. For the lung insert, the variation in the normalized HU values was relatively lower than that of the water insert as shown in Figure 8. Linac 1 showed a maximum variation of -11.2 ± 8.9 with minimal trend along the longitudinal axis of the phantom. A few outliers were also observed for Linac 2 toward the inferior end of the phantom. In addition to this, cortical bone showed a similar parabolic trend as observed in the case of water. All five Linac appeared to have close agreement in terms of variation from one end to the other, with a few outliers for Linac 5 close to the phantom center as shown in Figure 9.

Imaging modality comparison

The variations in mean HU values for multiple slices along the longitudinal axis of the AED phantom in FCT, Linac CBCT, and Gamma Knife CBCT for water, lung, and cortical bone inserts are shown in Figures 10-12, respectively. In each case, the yellow triangle represents the center of the scanned

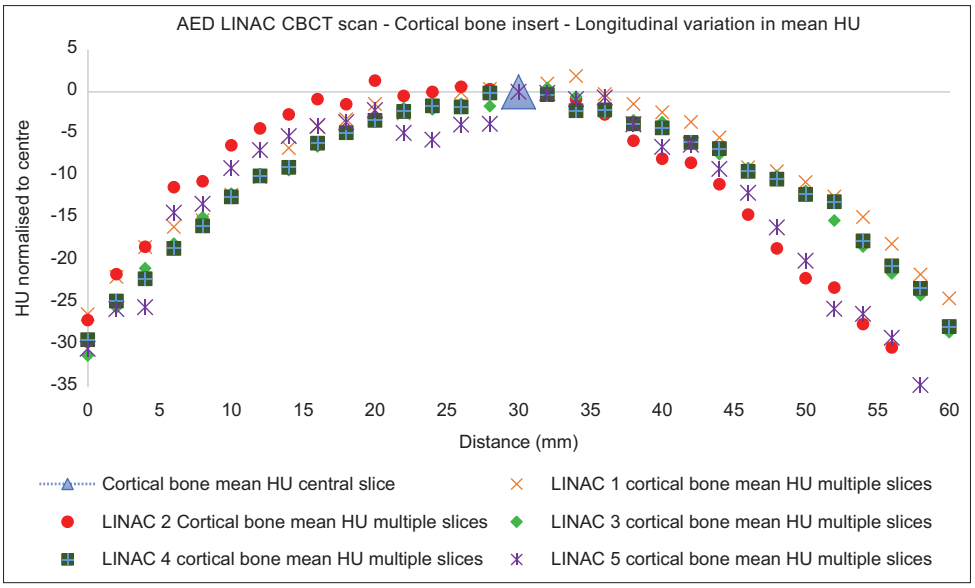

Figure 9: Variation in Linac CBCT HU values of Cortical bone insert along the longitudinal axis of the AED phantom. CBCT: Cone-beam computed tomography, AED: Advanced electron density, HU: Hounsfield unit

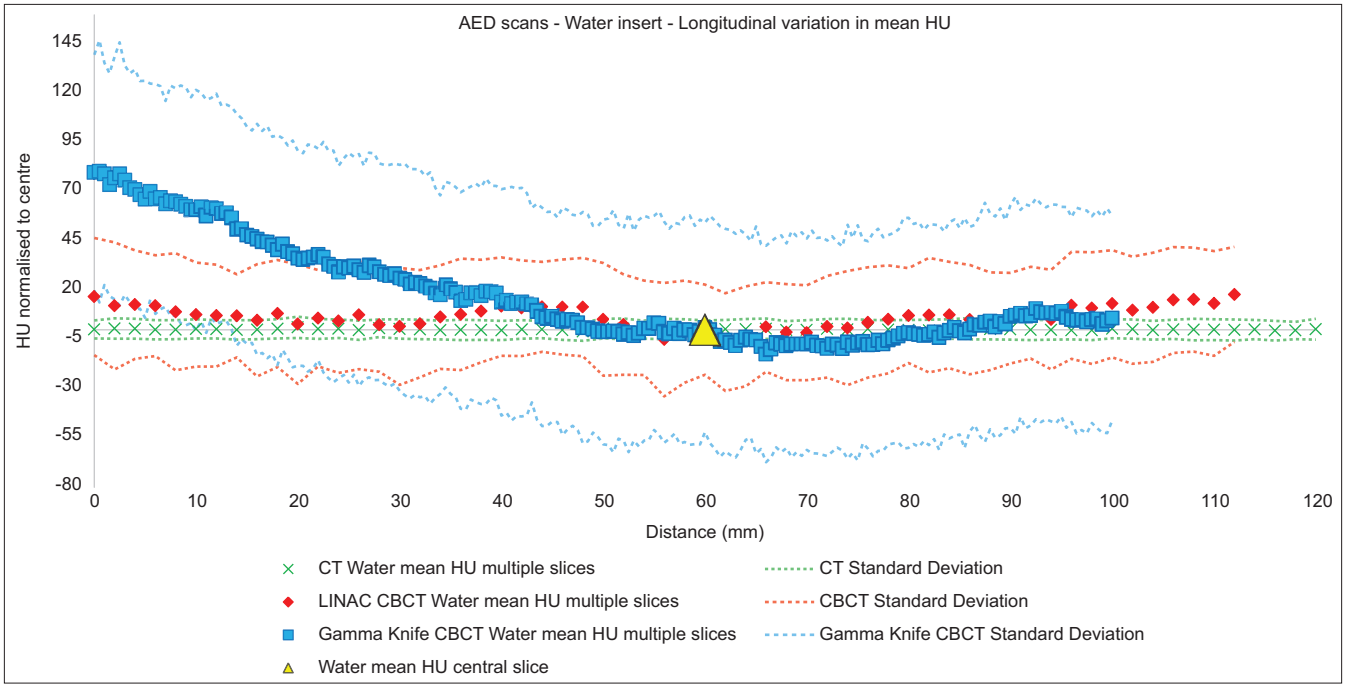

Figure 10: Variation in the HU values of water insert along the longitudinal axis of the AED phantom. AED: Advanced electron density, HU: Hounsfield unit

phantom. The HU value of respective insert along the phantom with 2 mm increment is shown with red diamonds and green crosses for Linac CBCT and FCT, respectively. The blue squares show the same for Gamma Knife CBCT with 0.5 mm increment, in addition to this, blue, red, and green dotted lines illustrate the standard deviation (±1 σ) for Gamma Knife CBCT, Linac CBCT, and CT. It can also be noticed that the phantom scan lengths are different in each modality, which was mainly due to the scan range limitations associated with the Gamma Knife CBCT. The abscissa illustrates the scanned length of the phantom in millimeters with zero representing the bottom side of the phantom (superior end). On the other hand, mean HU (normalized to the reading at the center of scanned part of the phantom for individual Linac) is plotted along the ordinate indicating the normalized HU values of each insert along the axial direction (i.e., in superior-inferior direction).

The maximum variation among the three modalities was observed in Gamma Knife CBCTs whereas FCT showed no significant deviation from the central value. In the case of

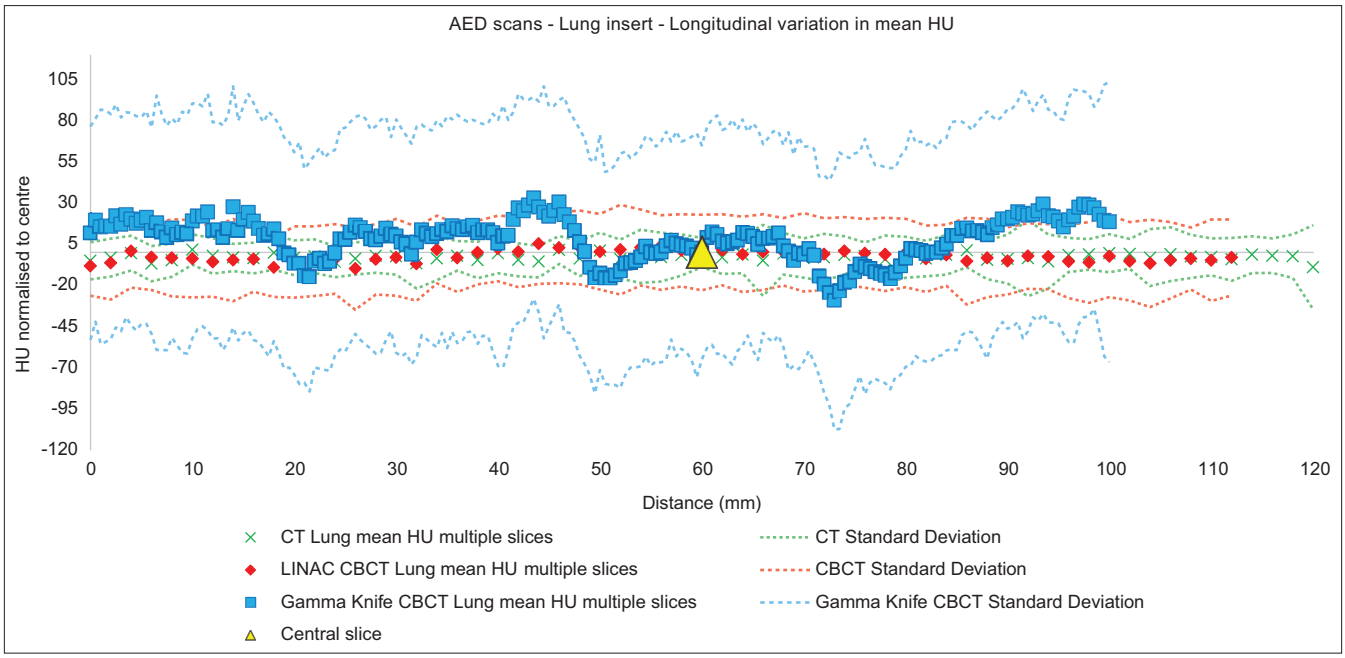

Figure 11: Variation in the HU values of lung insert along the longitudinal axis of the AED phantom. AED: Advanced electron density. HU: Hounsfield unit

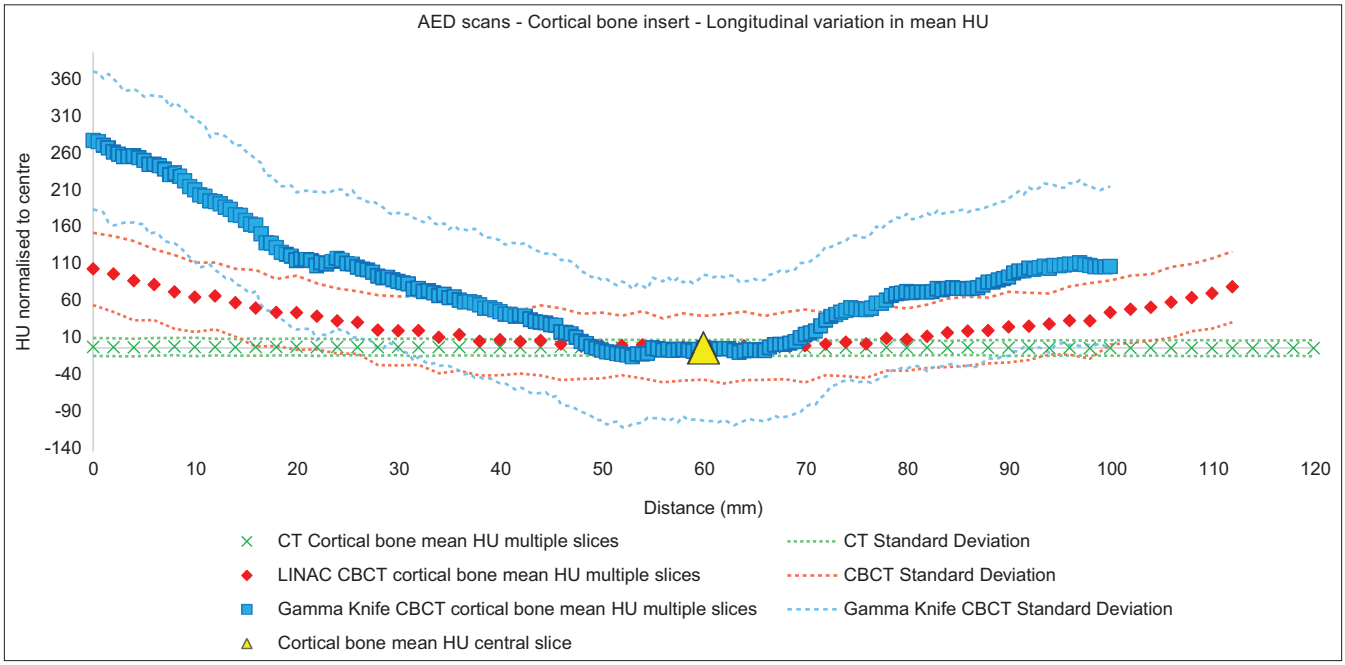

Figure 12: Variation in the HU values of cortical bone insert along the longitudinal axis of the AED phantom. AED: Advanced electron density. HU: Hounsfield unit

water insert, 79.41 ± 66.61 was the highest deviation noted for Gamma Knife CBCTs towards the superior region of the phantom [Figure 10], and it appeared to decrease along the longitudinal direction. However, in the case of the lung insert [Figure 11], the mean HU values fluctuated along the longitudinal axis unlike the water insert case, and the maximum value was calculated to be 33.18 ± 61.4, 43.5 mm away from the superior end. For cortical bone, a parabolic trend was observed for Gamma Knife CBCTs and Linac CBCTs and maximum deviation of 281.26 ± 93.52 was calculated towards the superior end of the phantom.

Dosimetric assessment of Hounsfield unit variations with different imaging modalities

PTV doses were analyzed on three different scans acquired on FCT, Linac CBCT XVI, and Gamma Knife CBCT. Table 3

Table 4: Planned target volume dose values calculated on different scans

Target	Volume (cm^3)	Minimum HU value	Maximum HU value	Mean HU value	SD
PTV FCT	106.23	889	1066	1038	22
PTV XVI	104.71	1020	1267	1169	27
PTV LGK	106.09	750	1561	1248	78

CT: Computed tomography, PTV: Planned target volume, FCT: Fan-beam CT, XVI: X-ray volumetric imaging, LGK: Leksell Gamma Knife Icon, HU: Hounsfield unit, SD: Standard deviation

Table 5: Planned target volumes dose analysis

Dose analysis	ROI type		
	PTV FCT	PTV XVI	PTV LGK
Minimum dose (Gy)	44.01	44.57	41.56
Maximum dose (Gy)	47.63	47.92	46.69
Mean dose (Gy)	46.65	47.03	45.56
SD (Gy)	0.64	0.55	0.69
Minimum DVH (PTV volume % receiving 90% of the maximum dose)	100	99.97	99.28
Maximum DVH (PTV volume % receiving 95% of the maximum dose)	95.94	96.81	93.87

CT: Computed tomography, PTV: Planned target volume, FCT: Fan-beam CT, XVI: X-ray volumetric imaging, LGK: Leksell Gamma Knife Icon, SD: Standard deviation, DVH: Dose-volume histogram, ROI: Region of interest

shows respective volume, minimum, mean and maximum HU values in the corresponding PTVs. The highest mean value was calculated to be 1248 for the PTV in Gamma Knife CBCT scan. In addition to this, Table 4 shows the dose analysis in all three scans. The mean dose in FCT and Linac CBCT scan differed by < 0.5 Gy whereas at least 1 Gy difference was observed between FCT and Gamma Knife CBCT as shown in Table 5.

Discussion

The Toshiba FCT generated consistent results whether a single or multi-slice methodology was used for HU value determinations, with similar mean values and standard deviations found across the length of modules, and minimal dependence on protocol selection. The intercomparison of linac-based CBCTs yielded significant differences in volumetric mean CT numbers for individual inserts, implying that machine specific HU to physical density calibrations would be required. Thus, differences were assessed by normalizing the CT number value to the central slice of the module. A similar trend in HU values was found across all inserts assessed, approximating a parabola with lower HU values toward the edges of the phantom. As normalization was required, calibrations specific to each linac-based cone beam CT would be required.

One should note that there are potentially several sources of variations in CT numbers for linac-based cone beam CTs acquired during radiotherapy treatment. CBCT protocols for Elekta XVI use separate imaging system geometries for the small, medium, and large field of view images, with the detector located in a different lateral position for each field of view. The imaging system can flex throughout gantry rotation, and this is corrected using flex measurements (maps) acquired for each field of view in clockwise and counter-clockwise gantry rotations. In addition, a variety of tube potentials, mAs values, and gantry rotation speeds can be used. Furthermore, partial arc images can be acquired in situations where patient collisions are an issue.

If linac-based CBCT images are to be used for dose calculations, such as for adaptive planning, making use of a consistent imaging protocol would ease quality assurance and improve confidence in dose calculations.[20] Ideally, this protocol could also be used for image guidance to optimize patient dose. Careful assessment of the quality of the CBCT would be required before clinical use for dose calculations, and an image assessment should be performed to identify any artifacts in the image or other discrepancies. Caution should be taken to assess whether the patient's contour is within the entirely within the field of view. Further analysis could be taken to assess the consistency of CT numbers in the lateral and vertical directions, and variations in CT numbers with the inserts in different positions in the phantom.

The Leksell Gamma Knife Icon CBCT exhibits very significant longitudinal dependence in HU values along the insert when compared to other imaging systems. The standard deviation of measured HU values was also significantly higher in comparison. This system can be utilized with preset protocols that use a specific scan geometry. All scans are acquired through a 200° arc, with a limited distance between the source, detector, and patient. Significant positional variations in HU with respect to position in the cone beam have been previously described.[19] Such differences limit the validity of using CT number information from the Icon CBCT for dose calculations. Artefacts in such images would need to be carefully assessed, as the Icon CBCT tends to generate an artefact at the superior end of the skull.

Dose statistics were assessed for a simple four-field conformal plan with a PTV. As the Leksell Gamma Knife Icon CBCT can be used on intracranial treatments, a PTV located in the brain was chosen for the dosimetric comparison. Dose statistics within the PTV exhibited general agreement when FCT and linac-based CBCT were used for dose calculation. Lower doses and coverage were found in dose calculations using the Icon CBCT. The assessment of the dataset indicated that this was primarily due to higher-than-expected HU values in the skull, leading to more attenuation in the plan. The International Atomic Energy Agency (IAEA) recommends a tolerance of ± 20 HU for all materials compared to the HU values specified by the manufacturer.[21] Our study shows that only FCT complies with the IAEA recommendations whereas linac CBCT and Icon-CBCT showed HU values outside the recommended tolerance.

Dosimetric comparisons could be expanded to other body sites, and the treatment techniques and the practical implementation

of adaptive planning using linac-based CBCT images should be rigorously commissioned. After optimization of a particular CBCT scan protocol for this purpose, scans acquired for IGRT can be compared with the planning CBCT to assess the accuracy of the CT number to density/electron density calibration and check for consistency of dose calculations. Such an approach could be phased in for sites using particular planning techniques and then expanded to other sites. A quality assurance program should be involved to assess image quality and adaptive plan quality. It is highly recommended to perform an end-to-end test before using any imaging modality for dose calculations. This study also recommends assessing the variation of HUs in the scan volume, in particular along the long axis.

Conclusion

This study shows that there is a minimal variation with FCT between single, volume-based, and multi-slice methods, and hence the current approach of determining the CT-ED curve based on a single-slice method would be sufficient for producing a HU calibrations curve for treatment planning. However, CBCTs acquired on linac, and in particular Gamma Knife systems show significant variations along the long axis, which is likely to affect the dose calculations performed on CBCTs, and it is highly recommended to assess the Hounsfield values on multiple slices before using the HU curve for dose calculations.

Financial support and sponsorship

Nil.

Conflicts of interest

There are no conflicts of interest.

References

1. Pereira GC, Traughber M, Muzic RF Jr. The role of imaging in radiation therapy planning: Past, present, and future. Biomed Res Int 2014;2014:231090.
2. Gardner SJ, Kim J, Chetty IJ. Modern radiation therapy planning and delivery. Hematol Oncol Clin North Am 2019;33:947-62.
3. An HJ, Son J, Jin H, Sung J, Chun M. Acceptance test and clinical commissioning of CT simulator. Prog Med Phys 2019;30:160-6.
4. Thomas SJ. Relative electron density calibration of CT scanners for radiotherapy treatment planning. Br J Radiol 1999;72:781-6.
5. Hussain A, Muhammad W. Treatment Planning in Radiation Therapy. In: Maqbool, M. (eds) An Introduction to Medical Physics. Biological and Medical Physics, Biomedical Engineering. Springer, Cham. 2017. p. 63-129. Available from: https://doi.org/10.1007/978-3-319-61540-0_4. [Last accessed on 2022 Nov 15].
6. Jaafar AM, Elsayed H, Khalil MM, Yaseen MN, Ammar H, Alshewered A. The influence of different kVs and phantoms on computed tomography number to relative electron density calibration curve for radiotherapy dose calculation. Precis Radiat Oncol 2022;6:289-97.
7. Chand B, Priyamvda, Kumar M, Prasher S, Kumar M. Effect of CT number to relative electron density curves acquired at different tube voltage and current on radiotherapy dose calculation. J Phys Conf Ser 2022;2267:012140. Available from: https://iopscience.iop.org/article/10.1088/1742-6596/2267/1/012140. [Last accessed on 2022 Nov 15].
8. Electron Density Phantom CIRS. Available from: https://www.cirsinc.com/products/radiation-therapy/electron-density-phantom/. [Last accessed on 2022 Nov 15].
9. Pro-rt-ed Diagnomatic. Available from: https://www.diagnomatic.com/devices/pro-rt-ed. [Last accessed on 2022 Nov 15].
10. Advanced Electron Density Phantom (GAMMEX™ Technology) – Sun Nuclear. Available from: https://www.sunnuclear.com/products/advanced-electron-density-phantom. [Last accessed on 2022 Nov 15].
11. Tissue Characterization Phantom Model 467 – CSP Medical. Available from: https://cspmedical.com/content/102-1492_tissue_phantom_user_guide.pdf. [Last accessed on 2022 Nov 15].
12. Posiewnik M, Piotrowski T. A review of cone-beam CT applications for adaptive radiotherapy of prostate cancer. Phys Med 2019;59:13-21.
13. Hatton J, McCurdy B, Greer PB. Cone beam computerized tomography: The effect of calibration of the Hounsfield unit number to electron density on dose calculation accuracy for adaptive radiation therapy. Phys Med Biol 2009;54:N329-46.
14. Ignjic T, Pavicar B, Kolarevic G, Ranogajec Z. Computer Tomography Tube Voltage and Phantom Dimensions Influence on the Number of Hounsfield Units. International Conference on Medical and Biological Engineering. Cham: Springer; 2020. p. 111-8.
15. Zurl B, Tiefling R, Winkler P, Kindl P, Kapp KS. Hounsfield units variations: Impact on CT-density based conversion tables and their effects on dose distribution. Strahlenther Onkol 2014;190:88-93.
16. Schröder L, Stankovic U, Sonke JJ. Technical Note: Long-term stability of Hounsfield unit calibration for cone beam computed tomography. Med Phys 2020;47:1640-4.
17. Yoo S, Yin FF. Dosimetric feasibility of cone-beam CT-based treatment planning compared to CT-based treatment planning. Int J Radiat Oncol Biol Phys 2006;66:1553-61.
18. Richter A, Hu Q, Steglich D, Baier K, Wilbert J, Guckenberger M, *et al.* Investigation of the usability of conebeam CT data sets for dose calculation. Radiat Oncol 2008;3:42.
19. Ramachandran P, Perrett B, Dancewicz O, Seshadri V, Jones C, Mehta A, *et al.* Use of GammaPlan convolution algorithm for dose calculation on CT and cone-beam CT images. Radiat Oncol J 2021;39:129-38.
20. Chen S, Le Q, Mutaf Y, Lu W, Nichols EM, Yi BY, *et al.* Feasibility of CBCT-based dose with a patient-specific stepwise HU-to-density curve to determine time of replanning. J Appl Clin Med Phys 2017;18:64-9.
21. IAEA. IAEA Human Health Series No. 19. Quality Assurance Programme for Computed Tomography: Diagnostic and Therapy Applications. Vienna, Austria: IAEA; 2012.